Abhijit Bhattacharyya[1]
Department of Mechanical Engineering,
École Centrale School of Engineering,
Mahindra University,
Hyderabad 500043, India
e-mail: diroindia@gmail.com

John K. Schueller
Department of Mechanical & Aerospace Engineering,
University of Florida,
Gainesville, FL 32611
e-mail: schuejk@ufl.edu

Brian P. Mann
Department of Mechanical Engineering & Materials Science,
Duke University,
Durham, NC 27708
e-mail: brian.mann@duke.edu

Tony L. Schmitz
Department of Mechanical, Aerospace & Biomedical Engineering,
University of Tennessee,
Knoxville, TN 37996
e-mail: tony.schmitz@utk.edu

Michael Gomez
Department of Mechanical, Aerospace & Biomedical Engineering,
University of Tennessee,
Knoxville, TN 37996
e-mail: mgomez5@vols.utk.edu

Uncertainty Propagation Through An Empirical Model of Cutting Forces in End Milling

Empirical mathematical models of cutting forces in machining processes use experimentally determined input parameters to make predictions. A general method for propagation of input parameter uncertainties through such predictive models is developed. Sources of uncertainty are identified and classified. First, a classical uncertainty procedure is employed to estimate uncertainties associated with the data reduction equation using a first-order Taylor series expansion. Small values of input parameter uncertainties justify this local linearization. Coverage factors required to estimate confidence intervals are computed based on appropriate underlying statistical distributions. A root sum of squares method yields the overall expanded uncertainty in force predictions. A popular model used for predicting cutting forces in end milling is selected to demonstrate the procedure, but the demonstrated approach is general. The analysis is applied to experimental data. Force predictions are quoted along with a confidence interval attached to them. An alternative analysis based on Monte Carlo simulations is also presented. This procedure yields different insights compared with the classical uncertainty analysis and complements it. Monte Carlo simulation provides combined uncertainties directly without sensitivity calculations. Classical uncertainty analysis reveals the impacts of random effects and systematic effects separately. This information can prompt the user to improve the experimental setup if the impact of systematic effects is observed to be comparatively large. The method of quoting an estimate of the uncertainty in force predictions presented in this paper will permit users to assess the suitability of given empirical force prediction models in specific applications. [DOI: 10.1115/1.4049508]

Keywords: cutting force uncertainty, cutting coefficient uncertainty, force model uncertainty

1 Introduction

End milling is a machining process which is widely used in the metalworking industry. Modeling of cutting forces in end milling is important for predicting power requirements while specifying milling equipment [1], analyzing the stability of the machining processes [2], analyzing surface location errors [2], and estimating the load on end mills [3]. A large number of predictive cutting force models for end milling are available in the literature [1,4].

It is usual to present a model along with experimental results that validate it. The current practice is usually to present the theoretical predictions and the experimental results on a common graph. A visual comparison is made, and the modeler then claims that the theory predicts the experimental results well. This practice is so ingrained in the community, that the question, "quantitatively, how good is the prediction?" is rarely asked.

The majority of the cutting force models are empirical, lumped parameter models [1,2,4]. The geometry of the process is captured analytically, and all other factors such as work material properties, friction effects, tool material effects, and tool wear effects are captured in lumped parameter form. Values of these lumped parameters are found by experimental measurements and used as inputs in the model to predict forces for any combination of machining parameters.

This document presents a technique that captures the uncertainties associated with measured values of the input parameters. These uncertainties are propagated through a popular empirical cutting force model. Predicted force values are accompanied by a quantitative statement of the prediction uncertainties corresponding to a specified confidence interval.

2 Force Prediction Model With Input Parameter Uncertainty

A specific form of a widely used empirical model for predicting cutting force components previously described by Tlusty [1] is reproduced in the Appendix A and B for ready reference and to clarify the terminology used here. The model applies to straight-flute end milling cutters. The axial force component vanishes. The feed force, F_x, and the lateral force, F_y, are the two relevant components in the plane where x–y is a rectangular coordinate system fixed to the machine. Components of the cutting force, $F_{x,y}$, are functions of input parameters that are either fixed or that have uncertainties associated with them, i.e., the data reduction equation (Eq. (B3) in the Appendix B) has the functional form

$$F_{x,y} = F_{x,y}\left(\underbrace{\lambda, D, b, z}_{\text{fixed}}, \underbrace{f_{T_i}, K_t, K_n}_{\text{uncertain}}\right) \tag{1}$$

where λ is the helix angle and is zero for a straight-flute cutter, D is the cutter diameter, b is the axial depth of cut, z is the number of teeth, f_{T_i} is the effective feed per tooth for the ith tooth, and K_t and K_n are the empirical cutting coefficients.

If f_{T_i}, K_t, and K_n could be measured directly, propagation of the associated uncertainties through the data reduction equation (1) would be a straightforward problem. However, the cutting coefficients are themselves variable, as shown in the Appendix B

[1]Corresponding author.

Manuscript received December 22, 2019; final manuscript received December 11, 2020; published online February 25, 2021. Assoc. Editor: Satish Bukkapatnam.

where cutting constants Γ_t, Ψ_t, Γ_n, and Ψ_n are defined. Uncertainties associated with cutting coefficients have to be deduced indirectly by first assessing the uncertainties associated with cutting constants. The effective feed per tooth is also measured indirectly. Thus, two more data reduction equations (Eqs. (B9) and (B10) in the Appendix B) are obtained having the functional forms

$$K_t, K_n = K_t, K_n\left(\underbrace{\bar{h}}_{\text{fixed}}, \underbrace{\Gamma_t, \Gamma_n, \Psi_t, \Psi_n}_{\text{uncertain}}\right) \text{ and}$$
$$f_{T_i} = f_{T_i}\left(\underbrace{f_T}_{\text{fixed}}, \underbrace{\rho}_{\text{uncertain}}\right) \tag{2}$$

where the commanded feed per tooth, f_T, and the average chip thickness, $\bar{h}$, are fixed quantities, whereas the radial runout over successive teeth, ρ, and the cutting constants, Γ_t, Γ_n, Ψ_t, and Ψ_n, are factors that have uncertainties associated with them.

The idea of quantifying uncertainties in cutting coefficients, for their propagation through models for stability and surface location analysis, has appeared in the literature [5,6]. However, the idea of quantifying variances in model input parameters for placing confidence intervals on predicted cutting forces and the determination of the variance-covariance matrix of cutting constants to capture the random effects for the logarithmic cutting coefficient model chosen here are contributions of this research. Capturing the error introduced in the effective feed per tooth due to radial runout is also a contribution of this research. The general approach to uncertainty propagation through the mathematical model is outlined in Fig. 1.

3 Sources of Uncertainty in Model Input Parameters and Their Classification by the Method of Evaluation

The sources of uncertainty in model input parameters are summarized in Table 1. The analytical method of uncertainty analysis presented in this research is based on the 1995 Guide to the Expression of Uncertainty in Measurement (GUM) [8]. The NIST Technical Note 1297 [7] is a more compact guideline authored by two of the primary authors [9] of the GUM and open to the general public. These documents classify uncertainties into the following:

(1) **Type A**: Uncertainty components evaluated by statistical methods
(2) **Type B**: Uncertainty components evaluated by other means

Measured values[2] of the lumped parameter cutting constants, γ_t, γ_n, ψ_t, and ψ_n, are subject to random effects owing to random variations in material properties, tool chip interface friction, etc., which can be quantified using statistical evaluation. The variances of the cutting constants, $\sigma^2(\gamma_t, \gamma_n, \psi_t, \psi_n)$, and their covariances, $\sigma(\gamma_{t,n}, \psi_{t,n})$, are estimated using a Type A evaluation.

The source of systematic errors are two measurement devices. The dynamometer, amplifier, and data acquisition card system form a chain used to obtain measured values of cutting force components, $f_{x,y}$. A dial indicator, having a finite resolution, has been used to obtain measured values of the radial runout of successive teeth, ρ. The effects of these two measuring devices on the variances of model input parameters are quantified using the Type B evaluation:

(1) **Type B1** analysis refers to evaluation of variances of measured forces
(2) **Type B2** analysis refers to evaluation of variances of measured radial runouts of successive teeth

Variances of the cutting constants, $\Gamma_{t,n}$ and $\Psi_{t,n}$, due to random effects are obtained directly by using the Type A evaluation. However, the variances of the cutting coefficients, $K_{t,n}$, and effective feed per tooth, f_{T_i}, due to the systematic effects are not obtained directly using the Type B evaluation, but are obtained indirectly. The measurement values that are directly affected by systematic errors are the measured values of average force components, $\bar{f}_{x,y}$, and the radial runouts, ρ. Type B1 and B2 evaluations yield the variances of these measurements as will be shown. These variances need to be propagated to the estimated values of cutting coefficients, $k_{t,n}$, and effective feeds per tooth, f_{T_i}.

Table 1 Sources of uncertainty[a] in measured values of input parameters

Input parameter	Source(s) of uncertainty	Symbols used for variance/ covariance
Cutting constants Γ_t, Γ_n, Ψ_t, Ψ_n	Random effect due to variations in work material properties, tool-chip interface friction, cutting fluid, etc. (Type A uncertainty component)	$\sigma^2(\gamma_t)$, $\sigma^2(\psi_t)$, etc., & $\sigma(\gamma_t, \psi_t)$, etc.
Cutting coefficients K_t, K_n	Systematic effect due to variations in measured values of average force components, $\bar{f}_{x,y}$, found using a multicomponent dynamometer having piezoelectric charge devices. (Type B1 uncertainty component)	$\sigma^2(k_t)$, $\sigma^2(k_n)$, and $\sigma^2(\bar{f}_{x,y})$
Cutter tooth radial runout ρ	Systematic effect due to measurement uncertainty in runout measurement owing to the use of a dial indicator. (Type B2 uncertainty component)	$\sigma^2(\rho)$

[a]Although the sources are identified as random or systematic (bias) in this table, the analysis in this document classifies them as Type A or Type B, based on the method of evaluation as suggested in the NIST document [7].

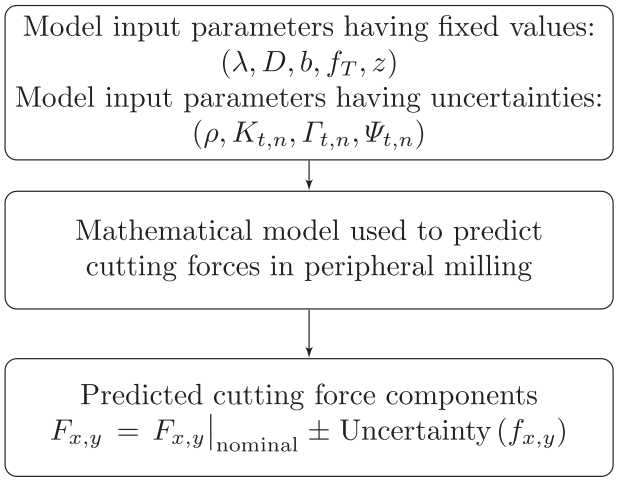

Fig. 1 The uncertainty propagation approach

4 Experimental Calibration of the Force Model

The cutting force model described in the Appendix B was experimentally calibrated. Measured values of the input parameters displayed in Fig. 1 are required to make force predictions.

[2]Lowercase representations, such as γ_t, γ_n, ψ_t, ψ_n, k_t, and k_n, are used to denote sample measures that are used as estimates of the corresponding population measures, Γ_t, Γ_n, Ψ_t, Ψ_n, K_t, and K_n, respectively.

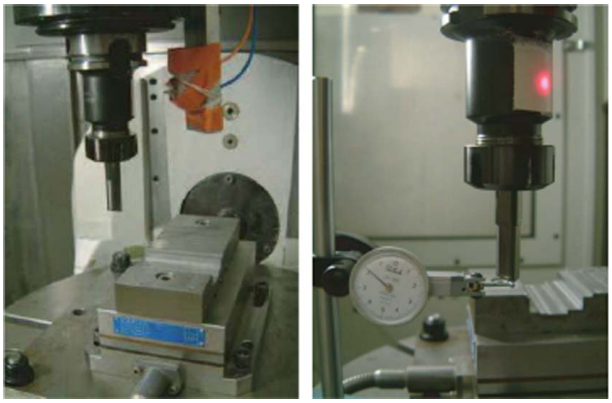

Fig. 2 Experimental setup showing the straight-flute endmill held in a collet chuck and mounted on the vertical spindle, the laser tachometer, and the workpiece mounted on the dynamometer that is held on the machine table. The setup for radial runout measurement using the dial indicator is also shown.

Table 2 Experimental setup description

Equipment	Make and model[a]	Description
Machine tool	Mikron – UCP-Vario	Five-axis machining center with hollow shank adaption HSK-63A and spring collet holding.
Cutting tool	SGS Catalog No. 30423	12.7 mm diameter, uncoated solid carbide endmill having two straight flutes.
Dynamometer	Kistler Catalog No. 9257B	Three-component dynamometer with charge amplifier
Dial gage	Teclock Catalog No. LT1-355	Lever-type dial indicator with least count 2.5 μm (0.0001 in.)
DAQ card	National Instruments	12-bit card used to acquire data at a sampling frequency of 60 kHz

[a]In this document, all commercial products are identified for the sake of completeness, and to enable other investigators to replicate the experiments. This does not constitute endorsement of any of these products.

4.1 The Partial Radial Immersion Experiment. Figure 2 shows the experimental setups for measurement of cutting forces and radial runout of cutter teeth. A description of these setups is outlined in Table 2. Fixed cutting conditions of 72 m/min cutting speed, 0.5 mm axial depth of cut, and 70 mm length of cut were used. A low carbon steel (HV170) workpiece was dry milled using a square end uncoated solid carbide endmill of diameter 12.7 mm having straight flutes with two equispaced teeth. The nominal total indicated reading (TIR) over the two teeth was found to be 15 μm using a dial indicator having least count 2.5 μm. A multicomponent dynamometer was used to record two components of the force in the plane, i.e., the feed force, F_x, and the lateral force, F_y.

Cutting coefficients were extracted based on a set of experiments with 25% radial immersion (RI). The average chip thickness was varied by changing the feed based on Eq. (B8). Values of cutting coefficients were recorded for each level of average chip thickness, and linear regression was used to establish relationships between them.

4.2 Experimental Extraction of Cutting Coefficients. Equations (B3) and (B7) point to correlation of the cutting coefficients. Hence, in addition to the variances of the tangential cutting coefficient, K_t, and the normal cutting coefficient, K_n, their covariances need to be estimated.

Experiments were conducted at seven different values of feed, in the range 0.050–0.250 mm/tooth, and the cutting force components were recorded in a fixed frame of reference. The measured average values of the feed force component, $\bar{f}_x$, and the lateral force component, $\bar{f}_y$, were computed.

At each feed rate, the experiment was repeated five times. Forces were averaged over one rotation, on a per tooth basis. The average was taken for two successive rotations, which reduces the variability. Values of K_t and K_n, corresponding to each feed rate, were derived using Eq. (B7). Seven sets of data, with five replications in each set, were collected for fitting a linear model according to Eq. (B9). Two parameters, the slope and the intercept, were fitted to 35 points in each regression resulting in 33 degrees-of-freedom [7] for the standard uncertainties associated with each of the four cutting constants Γ_t, Γ_n, Ψ_t, and Ψ_n.

Since the cutting constants of Eq. (B9) are to be estimated simultaneously, a multiresponse linear regression solution enables the evaluation of the variance-covariance matrix between the responses and the variance-covariance matrix of the random error in the regression model, which permits the extraction of the variance-covariance matrix of the cutting constants. This information is required for the evaluation of uncertainty from random effects in the measuring process for the cutting constants.

4.3 Estimation of Cutting Constants and Cutting Coefficients. For the simultaneous estimation of the cutting constants $\Gamma_{t,n}$ and $\Psi_{t,n}$, of Eq. (B9), a multi response model is necessary. Such a model has been proposed by Zellner [10] who has provided an example which shows how to estimate the multiple response parameters and obtain the variance-covariance matrix of these estimators. Kurdi [5] and Duncan et al. [6] have also used this model to solve a similar problem. Based on the Zellner's method, the fitted regression lines are displayed in Fig. 3. The estimated cutting constants, $\Gamma_{t,n}$ and $\Psi_{t,n}$, are calculated and listed in Table 3, and the corresponding variance-covariance matrix is displayed in Table 4.

The nominal values of cutting coefficients, obtained from the experiment, may be computed by using the nominal values of the cutting constants in the Eq. (B9), whereby

$$K_t = \exp(\Gamma_t)(\bar{h})^{\Psi_t} = 1312(\bar{h})^{-0.4145} \ (\mathrm{N/mm^2}) \tag{3}$$

$$K_n = \exp(\Gamma_n)(\bar{h})^{\Psi_n} = 1103(\bar{h})^{-0.5203} \ (\mathrm{N/mm^2}) \tag{4}$$

with the average chip thickness, $\bar{h}$, expressed in millimeters.

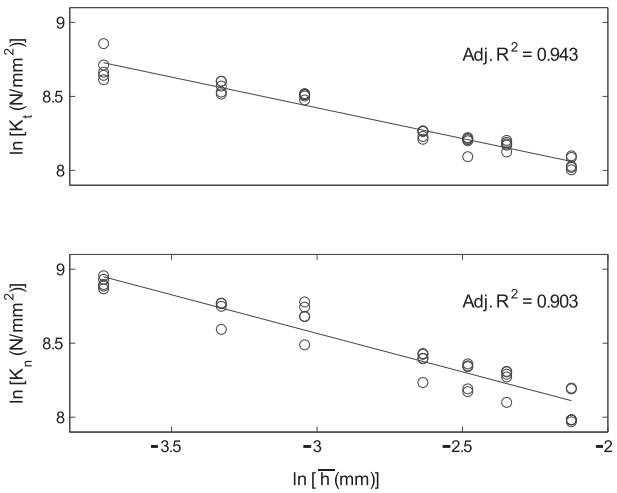

Fig. 3 Linear regression fitting of cutting coefficients, as a function of the average chip thickness, for dry milling of low carbon steel (HV170), using a straight-flute solid carbide endmill, having two equispaced teeth, and a nominal runout of 15 μm. Experimental points are denoted by small circles.

Table 3 Mean values of estimated cutting constants

	Γ_t	Ψ_t	Γ_n	Ψ_n
Estimates	7.179	−0.4145	7.006	−0.5203
Goodness of fit (Adj. R^2)	0.943		0.903	

Table 4 Variance-covariance matrix of cutting constants

	Γ_t	Ψ_t	Γ_n	Ψ_n
Γ_t	0.002561	0.000879	0.002046	0.000702
Ψ_t		0.000312	0.000702	0.000249
Γ_n			0.007161	0.002456
Ψ_n				0.000873

The above expressions are derived based on experiments in which the domain of $\bar{h}$ was

$$0.0239 \text{ (mm)} \leq \bar{h} \leq 0.1194 \text{ (mm)} \tag{5}$$

4.4 Variances of Cutting Constants, Average Forces, and Radial Runout. The two coefficients K_t and K_n are possibly correlated. Therefore, their covariance needs to be determined. The covariance of cutting coefficients due to random effects was not calculated directly because of the structure of the cutting coefficient model. Although the cutting coefficients are nonlinear functions of h (or $\bar{h}$), the linear relationship between the logarithms of $K_{t,n}$ and h (or $\bar{h}$) was exploited. This yields the variances and covariances of cutting constants (instead of cutting coefficients) by linear regression using the Zellner's [10] method. These variances quantify the random effects in the estimation of the cutting constants and are designated as having been evaluated using a Type A analysis.

The variances in measured values of average force components, $\sigma^2(\bar{f}_{x,y})$, may be calculated using a Type B2 evaluation based on estimates of standard uncertainties in force measurements provided by the manufacturer of the force measuring instrument [11]. The multicomponent dynamometer consists of piezoelectric charge devices. As per the instrument manufacturer's certificate, the uncertainty may be evaluated as follows assuming an underlying normal distribution for the variances

σ (force measurement):	0.5%
σ (charge measurement):	0.5%
Net $\sqrt{\sigma^2(\text{force}) + \sigma^2(\text{charge})}$:	0.707%
Add σ (charge amplifier):	0.5%
$\therefore \sigma(\bar{f}_{x,y}) \simeq 0.707\% + 0.5\%$:	1.207%

Based on this certificate provided by the ISO 17025 certified manufacturer, values of the standard uncertainty in measured values of the average force components, $\sigma(\bar{f}_{x,y})$, are set at 1.207% of the nominal values of the average force components, i.e.,

$$\sigma(\bar{f}_{x,y}) \simeq 0.01207 \bar{f}_{x,y} \tag{6}$$

The uncertainty associated with runout measurement is captured using a Type B2 evaluation as discussed in Ref. [7]. The dial indicator used in runout measurement resolves to 0.0025 mm. The lever-type indicator has a small cosine error that is neglected in this analysis. Based on a rectangular (uniform) distribution of the half-open interval, the variance of the radial runout measurement [7] is

$$\sigma^2(\rho) = \left(\frac{0.0025}{\sqrt{3}}\right)^2 \tag{7}$$

5 Uncertainty Analysis Based on the Classical Approach

The combined uncertainty, $\sigma_C(y)$, in the measured value, y, of a measurand, Y, which is obtained by measuring the values, x_i, of N input parameters, X_i, is considered to be the estimated standard deviation of y, and is given by [7]

$$\sigma_C(y) = \sqrt{\sum_{i=1}^{N} \left(\frac{\partial y}{\partial x_i}\right)^2 \sigma^2(x_i) + 2 \sum_{i=1}^{N-1} \sum_{j=i+1}^{N} \frac{\partial y}{\partial x_i} \frac{\partial y}{\partial x_j} \sigma(x_i, x_j)} \tag{8}$$

where $\sigma^2(x_i)$ are the variances and $\sigma(x_i, x_j)$ are the covariances of the measured input estimates. In writing Eq. (8), it has been assumed that the data reduction equation is

$$Y = Y(X_1, X_2, \ldots, X_N) \tag{9}$$

Taylor and Kuyatt [7] have explained that the relation described in Eq. (8) is based on a first-order Taylor expansion of the expression for Y given by the data reduction equation (9). The implication is that the values of input parameter uncertainties must be small enough so that local linearization may be justified.

Inspection of the values of the variances (Table 4) and comparison with the mean values of cutting constants (Table 3) show that the variances in measured values of the cutting constants are indeed small. Similarly, variances in measured values of average forces given by Eq. (6), and the variance of radial runout measurement given by Eq. (7), are also small. These pieces of data suggest that all the directly measured quantities in our experiments: cutting constants, average cutting forces, and radial runout, have variances which are small, compared with their individual nominal values.

There is another limitation to the use of the classical approach to uncertainty propagation as described by Eq. (8). The method works only if the data are real valued, i.e., it is only valid for the case of scalar data. If data are multivariate, the method does not apply. An example of such a case would be complex valued data which are encountered in frequency response function analysis. In our case, all the input parameters are scalar quantities.

The ISO GUM [8] does not require an extensive knowledge of the complete probability distribution functions for the input variables in order to apply Eq. (8). It propagates estimates of expected values and standard uncertainties for input parameters through a linear approximation of the measurement equation to yield an estimate and standard uncertainty for the value of the measurand. It applies as an approximation in those situations where reasonable estimates for the expected values and standard deviations are available [9]. We have reasonable estimates of input parameters and their variances. For all these reasons, application of Eq. (8) is justified.

Following the uncertainty analysis procedure as outlined in Taylor and Kuyatt [7], individual standard uncertainties are propagated through the model to obtain an estimate of the combined uncertainties. The combined uncertainty of predicted force components due to the random effects on cutting constants is designated $\sigma_{C_A}(f_{x,y})$. The combined uncertainty of force components due to the effect of the force measuring instrumentation is designated $\sigma_{C_{B1}}(f_{x,y})$, and that due to the runout measuring instrument is designated $\sigma_{C_{B2}}(f_{x,y})$.

Taylor and Kuyatt [7] refer to Eq. (8) as the law of propagation of uncertainty. The combined standard uncertainties of the predicted forces are derived using this law for which the functional relation "y" is given by Eq. (B3), which defines the function governing the force components. The sensitivity coefficients are the partial derivatives of the force components with respect to the model

input parameters which have uncertainties attached to them, namely, the cutting constants, the cutting coefficients, and the effective feed rates owing to radial runout of the cutter teeth upon mounting on the machine spindle.

6 Variances of Cutting Coefficients and Effective Feed Rates

In Sec. 4.4, it was observed that the variances of model input parameters due to random effects were directly available from Type A evaluation in the form of a variance-covariance matrix for the cutting constants $\Gamma_{t,n}$ and $\Psi_{t,n}$. However, the variances of model input parameters due to systematic effects were not available directly from Type B1 and B2 evaluations. Type B1 evaluation provided an estimate of the variances of the measured average forces (Eq. (6)), and Type B2 evaluation gave an estimate of the variances of measured values of radial runout of successive teeth (Eq. (7)). These variances need to be propagated to obtain estimates of the variances of cutting coefficients and effective feeds per tooth, which are model input parameters required for force predictions using Eq. (B3).

6.1 Propagation of Average Force Uncertainty to Cutting Coefficients. Equation (B7) yields the following sensitivity coefficients for use in propagation of the uncertainty in average force measurements to the uncertainties in cutting coefficients

$$\begin{Bmatrix} s_{tx} \\ s_{ty} \\ s_{nx} \\ s_{ny} \end{Bmatrix} = \begin{Bmatrix} \partial K_t/\partial \overline{F}_x \\ \partial K_t/\partial \overline{F}_y \\ \partial K_n/\partial \overline{F}_x \\ \partial K_n/\partial \overline{F}_y \end{Bmatrix} = \frac{2(\theta_{ex}-\theta_{st})}{af_T(\mu^2+\nu^2)} \begin{Bmatrix} \mu \\ \nu \\ \nu \\ -\mu \end{Bmatrix} \tag{10}$$

Using the above sensitivities in Eq. (8), the variances of cutting coefficients, due to the systematic effects, can be obtained

$$\begin{bmatrix} \sigma^2(k_t) \\ \sigma^2(k_n) \end{bmatrix} = \begin{pmatrix} s_{tx}^2 & s_{ty}^2 \\ s_{nx}^2 & s_{ny}^2 \end{pmatrix} \begin{Bmatrix} \sigma^2(\bar{f}_x) \\ \sigma^2(\bar{f}_y) \end{Bmatrix} \tag{11}$$

The values of $\sigma(\bar{f}_{x,y})$ in the Eq. (11) above are set at 1.207% of the nominal values of the average force components based on the instrument manufacturer's estimates, as detailed in Sec. 4.4. For simplicity, any possible correlation between K_t and K_n from measurement channel cross talk is neglected, i.e., $\sigma(k_t, k_n)$ is set to zero.

6.2 Propagation of Radial Runout Uncertainty to Effective Feeds. Equations (B10) yield the following sensitivity coefficients for use in propagation of the uncertainty in relative runout to the uncertainties in effective feeds

$$\frac{\partial f_{T_1}}{\partial \rho} = 1 \quad \text{and} \quad \frac{\partial f_{T_2}}{\partial \rho} = -1 \tag{12}$$

Equations (7) and (12) may be used in Eq. (8) to estimate the variances of the effective feed for each individual tooth

$$\sigma^2(f_{T_1}) = \left(\frac{\partial f_{T_1}}{\partial \rho}\right)^2 \sigma^2(\rho) = \left(\frac{0.0025}{\sqrt{3}}\right)^2 \tag{13}$$

$$\sigma^2(f_{T_2}) = \left(\frac{\partial f_{T_2}}{\partial \rho}\right)^2 \sigma^2(\rho) = \left(\frac{0.0025}{\sqrt{3}}\right)^2 \tag{14}$$

7 Propagation of Uncertainties Through the Cutting Force Model

The three components of uncertainty in input parameters have to be propagated through the force model equation (B3).

7.1 Sensitivity Coefficients of Component Uncertainties. Sensitivity coefficients used to determine Type A component uncertainties are

$$\begin{Bmatrix} s_{11} \\ s_{12} \\ s_{13} \\ s_{14} \\ s_{21} \\ s_{22} \\ s_{23} \\ s_{24} \end{Bmatrix} = \begin{Bmatrix} \partial F_x/\partial \Gamma_t \\ \partial F_x/\partial \Psi_t \\ \partial F_x/\partial \Gamma_n \\ \partial F_x/\partial \Psi_n \\ \partial F_y/\partial \Gamma_t \\ \partial F_y/\partial \Psi_t \\ \partial F_y/\partial \Gamma_n \\ \partial F_y/\partial \Psi_n \end{Bmatrix} = \frac{bf_T}{2} \begin{Bmatrix} K_t \sin 2\theta_p \\ [K_t \ln \bar{h}] \sin 2\theta_p \\ K_n(1-\cos 2\theta_p) \\ [K_n \ln \bar{h}](1-\cos 2\theta_p) \\ K_t(1-\cos 2\theta_p) \\ [K_t \ln \bar{h}](1-\cos 2\theta_p) \\ -K_n \sin 2\theta_p \\ -[K_n \ln \bar{h}] \sin 2\theta_p \end{Bmatrix} \tag{15}$$

where K_t and K_n are parameterized in $\Gamma_{t,n}$ and $\Psi_{t,n}$, according to Eq. (B9).

Sensitivity coefficients with respect to the cutting coefficients are used in the determination of the Type B1 component uncertainties and may be found using Eq. (B3).

$$\begin{Bmatrix} s_{x_{Kt}} \\ s_{x_{Kn}} \\ s_{y_{Kt}} \\ s_{y_{Kn}} \end{Bmatrix} = \begin{Bmatrix} \partial F_x/\partial K_t \\ \partial F_x/\partial K_n \\ \partial F_y/\partial K_t \\ \partial F_y/\partial K_n \end{Bmatrix} = \frac{bf_T}{2} \begin{Bmatrix} \sin 2\theta_p \\ 1-\cos 2\theta_p \\ 1-\cos 2\theta_p \\ -\sin 2\theta_p \end{Bmatrix} \tag{16}$$

Sensitivity coefficients with respect to the effective feeds are used in the determination of Type B2 component uncertainties. These are found using Eqs. (B3), (B8), and (B9)

$$\begin{Bmatrix} s_{xf} \\ s_{yf} \end{Bmatrix} = \begin{Bmatrix} \partial F_x/\partial f_T \\ \partial F_y/\partial f_T \end{Bmatrix} = \frac{b}{2} \begin{pmatrix} \sin 2\theta_p & 1-\cos 2\theta_p \\ 1-\cos 2\theta_p & -\sin 2\theta_p \end{pmatrix} \times \begin{Bmatrix} (1+\Psi_t)K_t \\ (1+\Psi_n)K_n \end{Bmatrix} \tag{17}$$

The sensitivities in Eqs. (15)–(17) are functions of the angular position of the pth tooth, θ_p. For illustrative purposes, they are plotted in Fig. 4 for a particular combination of machining parameters.

7.2 Combined Uncertainties of Type A. Let $\gamma_{t,n}$ and $\psi_{t,n}$ be the input estimates for the values of the cutting constants $\Gamma_{t,n}$ and $\Psi_{t,n}$, respectively, which are available from Table 3.

The estimated variances and the estimated covariances of the cutting constants are available from Table 4. These uncertainties have to be propagated to the predicted forces using the sensitivities, s_{ij}, given by Eq. (15).

These sensitivities are themselves a function of the cutting constants. Hence, they are evaluated at the estimated parameters $\gamma_{t,n}$ and $\psi_{t,n}$. The combined component uncertainties of predicted forces for the pth tooth, $\sigma_{C_A}(f_{x,y})$, due to the uncertainties in the cutting constants, are obtained using the sensitivities, s_{ij}, in the propagation law equation (8) which assumes the following form:

$$\begin{Bmatrix} \sigma^2_{C_A}(f_x) \\ \sigma^2_{C_A}(f_y) \end{Bmatrix} = \begin{pmatrix} s_{11}^2 & s_{12}^2 & s_{13}^2 & s_{14}^2 \\ s_{21}^2 & s_{22}^2 & s_{23}^2 & s_{24}^2 \end{pmatrix} \begin{Bmatrix} \sigma^2(\gamma_t) \\ \sigma^2(\psi_t) \\ \sigma^2(\gamma_n) \\ \sigma^2(\psi_n) \end{Bmatrix} + 2 \begin{pmatrix} s_{11}s_{12} & s_{11}s_{13} & s_{11}s_{14} & s_{12}s_{13} & s_{12}s_{14} & s_{13}s_{14} \\ s_{21}s_{22} & s_{21}s_{23} & s_{21}s_{24} & s_{22}s_{23} & s_{22}s_{24} & s_{23}s_{24} \end{pmatrix} \times \begin{Bmatrix} \sigma(\gamma_t,\psi_t) \\ \sigma(\gamma_t,\gamma_n) \\ \sigma(\gamma_t,\psi_n) \\ \sigma(\psi_t,\gamma_n) \\ \sigma(\psi_t,\psi_n) \\ \sigma(\gamma_n,\psi_n) \end{Bmatrix} \tag{18}$$

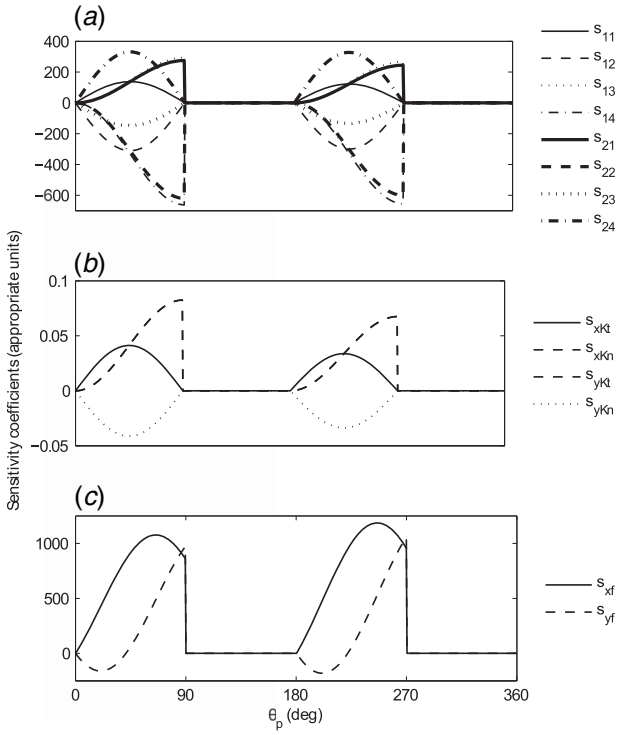

Fig. 4 Variation of sensitivity coefficients with angular position of the *p*th tooth: feed 0.150 mm/tooth, 50% radial immersion, up-milling, nominal runout 15 μm. Other conditions as in Table 5.

7.3 Combined Uncertainties of Type B1. The variances of cutting coefficients due to average force measurement uncertainties are available from Eq. (17) based on Type B2 evaluation. These uncertainties may be propagated to the predicted forces using Eq. (B3), and the sensitivities expressed in Eq. (16), to yield the combined component uncertainties of predicted forces for the *p*th tooth by applying Eq. (8)

$$\begin{Bmatrix} \sigma^2_{C_{B_1}}(f_x) \\ \sigma^2_{C_{B_1}}(f_y) \end{Bmatrix} = \begin{pmatrix} s^2_{xKt} & s^2_{xKn} \\ s^2_{yKt} & s^2_{yKn} \end{pmatrix} \begin{Bmatrix} \sigma^2(k_t) \\ \sigma^2(k_n) \end{Bmatrix} \tag{19}$$

7.4 Combined Uncertainties of Type B2. The uncertainties in effective feed per tooth due to radial runout measurement uncertainties are available from Eqs. (13) and (14) based on Type B2 evaluation. These uncertainties may be propagated to the predicted forces using Eq. (B3) and the sensitivities expressed in Eq. (11) to yield the combined component uncertainties of predicted forces for the *p*th tooth using Eq. (8)

$$\begin{Bmatrix} \sigma^2_{C_{B_2}}(f_x) \\ \sigma^2_{C_{B_2}}(f_y) \end{Bmatrix} = \sigma^2(f_T) \begin{Bmatrix} [s_{xf}]^2 \\ [s_{yf}]^2 \end{Bmatrix} \tag{20}$$

where the subscript on f_{T_p} is dropped for convenience.

8 Expanded Uncertainty

To specify the 95% confidence intervals on predicted forces, coverage factors for component expanded uncertainties are first computed based on the associated probability distributions of the component combined uncertainties. To determine the appropriate coverage factor for expanded uncertainty corresponding to a 95% confidence interval, an appropriate convolution of the various probability distributions needs to be considered [12,13].

8.1 Expanded Uncertainty Coverage Factor Type A. Type A standard uncertainty components, owing to the variances and covariances in the cutting constants, are combined using the law of propagation of uncertainty to yield the combined standard uncertainties, $\sigma_{C_A}(f_x)$ and $\sigma_{C_A}(f_y)$, which are assumed to have an approximately normal distribution. This happens when the conditions of the central limit theorem are met. When this is the case, $\sigma_{C_A}(f_{x,y})$ themselves have negligible uncertainty [7], and a $\pm 2\,\sigma_{C_A}(f_{x,y})$ width about the nominal value defines an interval in which the measurement result is believed to lie with a level of confidence of approximately 95%, i.e., the coverage factor for the expanded uncertainty is $\kappa_A = 2$.

If $\sigma_{C_A}(f_{x,y})$ themselves have non-negligible uncertainty, a conventional procedure may be used to produce a coverage factor that produces an interval having the approximate level of confidence desired. The effective degrees-of-freedom for the combined uncertainties are estimated based on the Welch–Satterthwaite (W–S) expression [7] as follows:

$$\mathrm{df}_{\mathrm{eff}}\big|_{\sigma_{C_A}(f_x)} = \frac{\sigma^{\star 4}_{C_A}(f_x)}{\dfrac{s^4_{11}\sigma^4(\gamma_t)}{df\,|_{\sigma(\gamma_t)}} + \dfrac{s^4_{12}\sigma^4(\psi_t)}{df\,|_{\sigma(\psi_t)}} + \dfrac{s^4_{13}\sigma^4(\gamma_n)}{df\,|_{\sigma(\gamma_n)}} + \dfrac{s^4_{14}\sigma^4(\psi_n)}{df\,|_{\sigma(\psi_n)}}} \tag{21}$$

$$\mathrm{df}_{\mathrm{eff}}\big|_{\sigma_{C_A}(f_y)} = \frac{\sigma^{\star 4}_{C_A}(f_y)}{\dfrac{s^4_{21}\sigma^4(\gamma_t)}{df\,|_{\sigma(\gamma_t)}} + \dfrac{s^4_{22}\sigma^4(\psi_t)}{df\,|_{\sigma(\psi_t)}} + \dfrac{s^4_{23}\sigma^4(\gamma_n)}{df\,|_{\sigma(\gamma_n)}} + \dfrac{s^4_{24}\sigma^4(\psi_n)}{df\,|_{\sigma(\psi_n)}}} \tag{22}$$

and

$$\mathrm{df}_{\mathrm{eff}}\big|_{\sigma_{C_A}(f_{x,y})} \leqslant \mathrm{df}|_{\sigma(\gamma_t)} + \mathrm{df}|_{\sigma(\psi_t)} + \mathrm{df}|_{\sigma(\gamma_n)} + \mathrm{df}|_{\sigma(\psi_n)} \tag{23}$$

where $\mathrm{df}_{\mathrm{eff}}\big|_{\sigma_{C_A}(f_x)}$ and $\mathrm{df}_{\mathrm{eff}}\big|_{\sigma_{C_A}(f_y)}$ are the effective degrees-of-freedom for the combined Type A component uncertainties of the measured values of the cutting force components, f_x and f_y, respectively. The superscript *, used in the terms $\sigma^\star_{C_A}(f_{x,y})$ in Eqs. (21) and (22), indicates that no correlation is considered among the inputs in calculating these combined uncertainties, i.e., the covariance terms in Eq. (18) are not considered, as suggested by Willink [14] in his generalization of the W–S expression for use with correlated uncertainty components.

The coverage factor for Type A component expanded uncertainty is determined based on the Student's *t*-distribution for any desired confidence interval and may be read off Table B1 in Ref. [7] knowing the value of $\mathrm{df}_{\mathrm{eff}}\big|_{\sigma_{C_A}(f_{x,y})}$. The effective degrees-of-freedom are functions of the angular position of the *p*th tooth, θ_p. Therefore, the coverage factor is also a function of θ_p. The functional dependence is illustrated for an example case in Fig. 5. For this particular case, it may be noted that the effective degrees -of-freedom is quite large ($\geq$31), so that the coverage factor approaches 2. By inspection of the Fig. 5, $\kappa_A \simeq 2.04$ may be taken as a good conservative value of the coverage factor for Type A component expanded uncertainty for a 95% confidence interval for both the *x* and *y* components of the force.

8.2 Expanded Uncertainty Coverage Factor Type B1. For Type B1 uncertainties due to systematic effects in the force measuring chain, underlying approximately normal distributions are assumed for the combined component uncertainties. Based on this the coverage factor for Type B1 component expanded uncertainty is $\kappa_{B_1} \simeq 2$ for a 95% confidence interval.

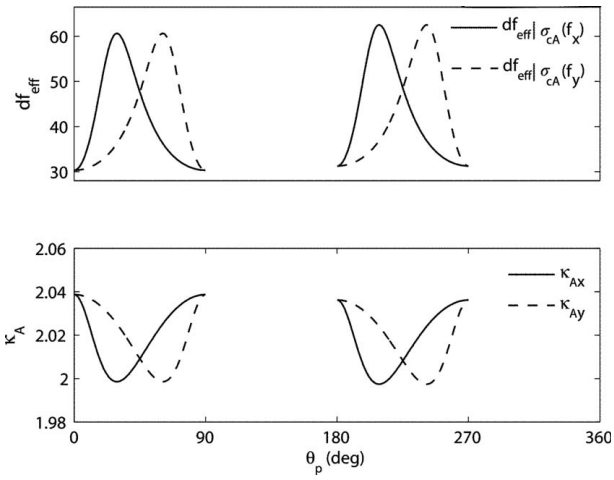

Fig. 5 Variation of the effective degrees-of-freedom of combined uncertainties of Type A, and the corresponding coverage factor, κ_A, for a 95% confidence interval, with angular position of the pth tooth: feed 0.150 mm/tooth, 50% radial immersion, up-milling, runout 15 μm. Other conditions as in Table 5.

Table 5 Experimental conditions used for verification of force predictions with a 12.7 mm diameter, 2-fluted endmill, cutting mild steel at speed 72 m/min speed, and axial depth of cut 0.5 mm

Results displayed in	Feed (mm/tooth)	Radial immersion	Up-, down- or mixed mode (RI > 0.5) milling
Fig. 8	0.150	50%	Up-milling
Fig. 9	0.050	50%	Up-milling
Fig. 10	0.150	75%	Mixed mode with $h = 0$ at the entry

8.3 Expanded Uncertainty Coverage Factor Type B2. For Type B2 uncertainties due to systematic effects of the runout measuring device, the rectangular distribution is assumed with infinite degrees-of-freedom owing to the fact that a single measurement is used. Based on this the coverage factor for the Type B2 component expanded uncertainty is $\kappa_{B_2} \simeq 1.65$ for a 95% confidence interval.

8.4 Overall Expanded Uncertainty. This problem has both Type A and Type B uncertainties with different types of underlying probability distributions (approximately normal and rectangular). To calculate the overall expanded uncertainty, a convolution of these probability distributions has to be considered, which is a difficult problem. According to the ISO GUM [8], Type A and Type B evaluations can be logically combined. Turzeniecka [12] has suggested various approximate methods of calculating the expanded uncertainty in such situations. The best choice depends on the relative magnitudes of Type A and Type B uncertainties. In the problem at hand, this ratio is not fixed. This fact is clarified with an example shown in Fig. 6. Moreover, the ratio is a function of the angular position of the pth tooth, θ_p, and process parameters such as the feed and radial immersion. For such a situation, Turzeniecka [12] has suggested the vector sum method, i.e., the root sum of squares (RSS) method as a good solution. The overall expanded uncertainty, $U(f_{x,y})$ is the RSS of the component expanded uncertainties

$$U(f_{x,y}) = \sqrt{\kappa_A^2 \sigma_{C_A}^2(f_{x,y}) + \kappa_{B_1}^2 \sigma_{C_{B1}}^2(f_{x,y}) + \kappa_{B_2}^2 \sigma_{C_{B2}}^2(f_{x,y})} \tag{24}$$

The predicted nominal forces, $F_{x,y}$, are quoted with an accompanying uncertainty, $\pm\Sigma(f_{x,y})$, corresponding to a specified confidence interval, where $F_{x,y}$ are calculated based on Eq. (B3).

The above analysis considers the forces and uncertainties associated with the engagement of a single tooth. For multiple tooth engagement, the forces due to each tooth are merely summed. However, the uncertainties must be obtained by the root sum of

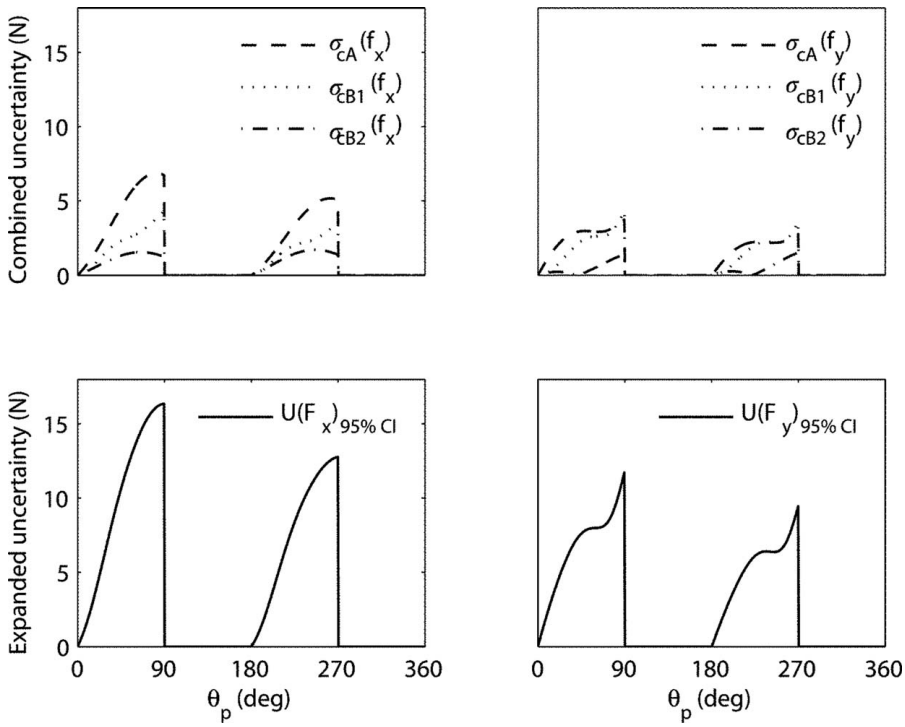

Fig. 6 Variation of component combined uncertainties, and overall expanded uncertainty for a 95% confidence interval, with angular position of the pth tooth: feed 0.150 mm/tooth, 50% radial immersion, up-milling, runout 15 μm. Other conditions as in Table 5.

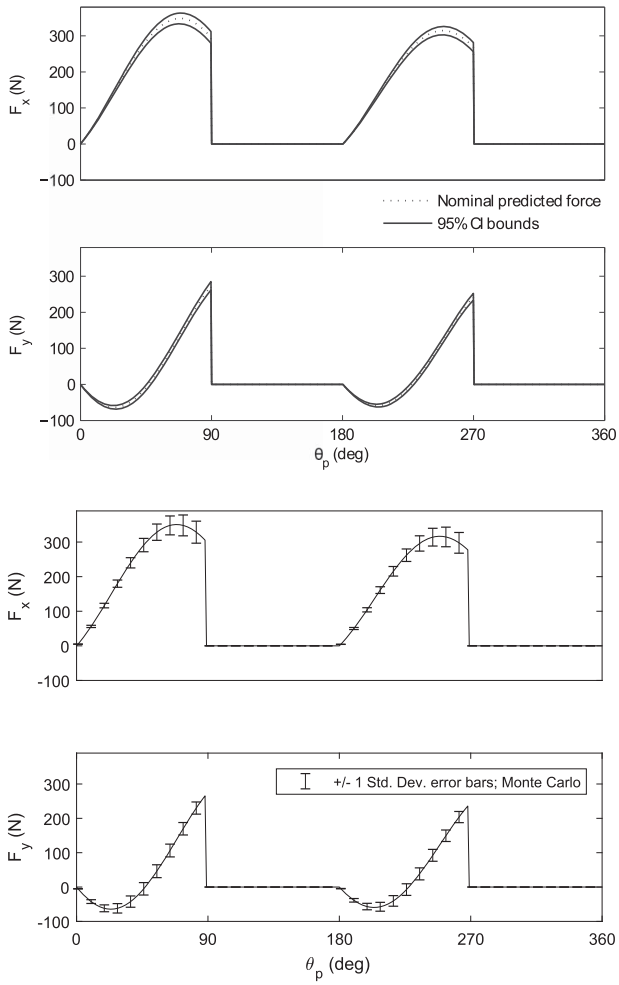

Fig. 7 Illustration of 95% confidence interval bounds on predicted cutting forces using classical uncertainty (upper panels) and error bar placement on predicted forces by Monte Carlo simulation (lower panels): feed 0.150 mm/tooth, 50% radial immersion, up-milling, runout 15 μm. Other conditions as in Table 5.

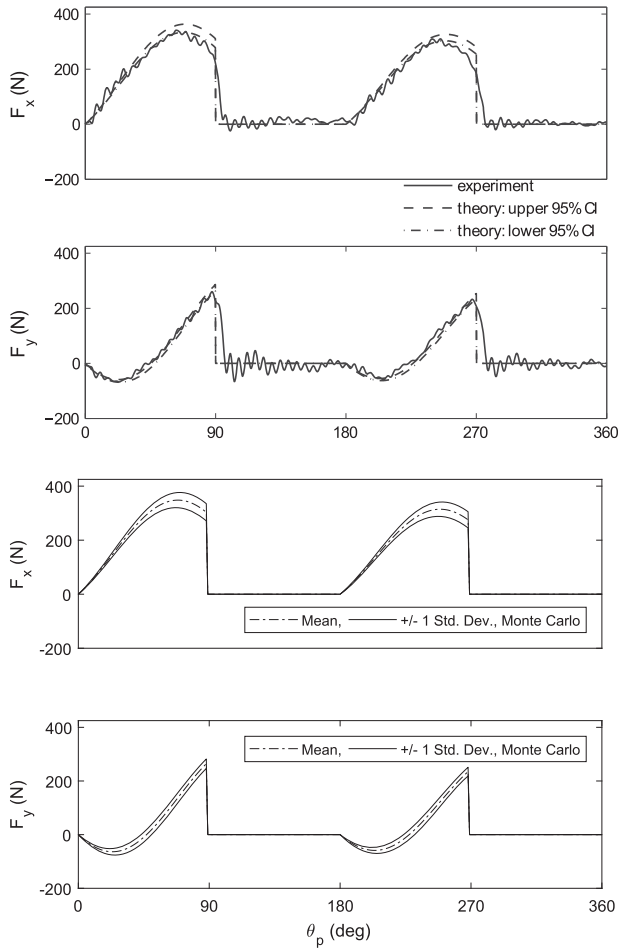

Fig. 8 Predicted versus experimental forces: feed 0.150 mm/tooth, 50% radial immersion, up-milling. Runout 15 μm. Other conditions as in Table 5. Comparison of classical uncertainty analysis (the top panels) with Monte Carlo simulations (the bottom panels).

squares method by considering the sum of the squares of each of the component combined uncertainties for every tooth individually and taking the square root of this overall sum.

All the uncertainties, combined as well as expanded, are functions of the angular position of the pth tooth, θ_p, an example of which is given in Fig. 6. For this same example, confidence intervals are placed on predicted forces and shown in the top two panels in Fig. 7.

9 Uncertainty Analysis Based on Inferential Statistics

To complement the classical uncertainty analysis presented in the earlier part of this paper, an alternative approach is proposed which is based on inferential statistics: the Monte Carlo simulation. This method offers a quick assessment of the estimated error in force prediction once the numerical values of input parameters and their variances are determined from experiment.

Values of input parameters and their variances are available from experimental results. Mean values of cutting constants are available from Table 3 and their variances from Table 4. The variances of effective feed for individual teeth are available from Eqs. (13) and (14) which return the same numerical value as the variance in radial runout obtained in Eq. (7). The reason is that effective feeds of individual teeth are linearly related to radial runout with unit sensitivities as seen in Eq. (12).

With the known values of input parameters and their variances, a Monte Carlo simulation is run using the analytical equations describing the cutting force components (5000 iterations for results presented in this paper). Values of the input parameters are varied individually in each iteration based on the individual standard deviation using a pseudorandom number generator available in commercial software. For cutting coefficients (alternatively, cutting constants), pseudorandom numbers are drawn from an approximately normal distribution, whereas for the radial runout they are drawn from a rectangular distribution. The result may be displayed by plotting mean values of predicted forces with a one standard deviation error band. An alternative way of displaying the Monte Carlo simulation results is to show predicted force values using the one standard deviation variation error bars as shown bottom two panels in Fig. 7.

The contributions of individual input parameters to variability of predicted cutting forces is assessed using the Monte Carlo simulation by varying only that input parameter while holding other input parameters to their mean values. A visual estimate of the contribution of each input parameter may be made by plotting the frequency distributions of predicted force components at some selected cutter rotation angle. For instance, one may choose the cutter rotation angle at which a force component has a peak value. It is noted that the feed force and lateral force peak at different cutter rotation angles. An example of this type of visualization is presented in Sec. 11.

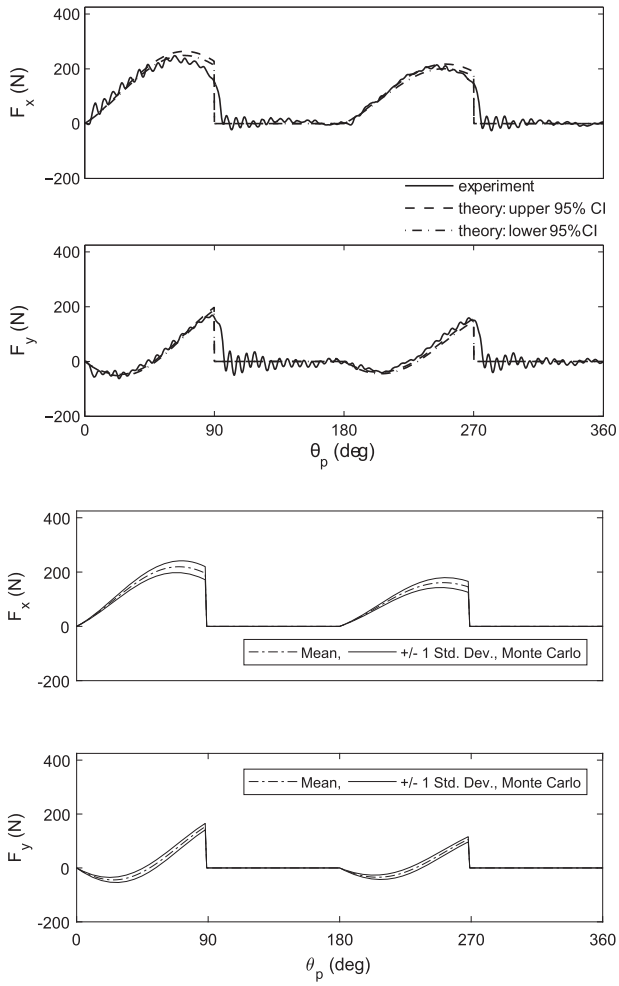

Fig. 9 Predicted versus experimental forces: feed 0.050 mm/tooth, 50% radial immersion, up-milling. Runout 15 μm. Other conditions as in Table 5. Comparison of classical uncertainty analysis (the top panels) with Monte Carlo simulations (the bottom panels).

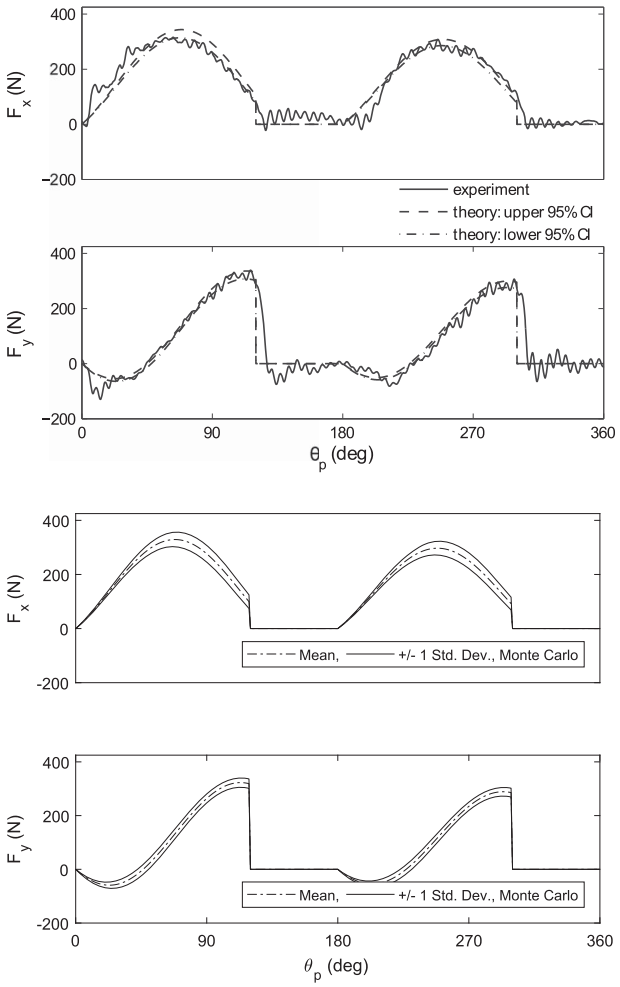

Fig. 10 Predicted versus experimental forces: feed 0.150 mm/tooth, 75% radial immersion, $h = 0$ at entry. Runout 15 μm. Other conditions as in Table 5. Comparison of classical uncertainty analysis (the top panels) with Monte Carlo (the bottom panels).

Certain characteristics of the Monte Carlo simulations presented here are worth noting. Covariances of cutting coefficients have been ignored in the analysis. The uncertainty contributors propagating through the cutting force equations directly yield the combined uncertainties in the predicted force values. A comprehensive analysis to determine combined uncertainties is not warranted.

10 Force Prediction With Uncertainty Bounds

Various combinations of radial immersion and feed rates were used to make force predictions for up milling (50% *RI*) and mixed mode (75% *RI*) using different values of feed as shown in Table 5. Confidence intervals were placed on predicted forces based on the classical uncertainty analysis, and one standard deviation error bounds were placed about the mean predicted force based on Monte Carlo simulations. Experimental force signals are superimposed on the predicted force signals to display the results graphically in Figs. 8–10. In each of these figures, the top two panels illustrate the placement of 95% confidence intervals on predicted forces based on the classical uncertainty approach, and the two lower panels display the +/- one standard deviation bounds about the mean predicted force based on the Monte Carlo approach. Experimental results are superimposed on the top two panels alone. Additional results are documented in Ref. [15].

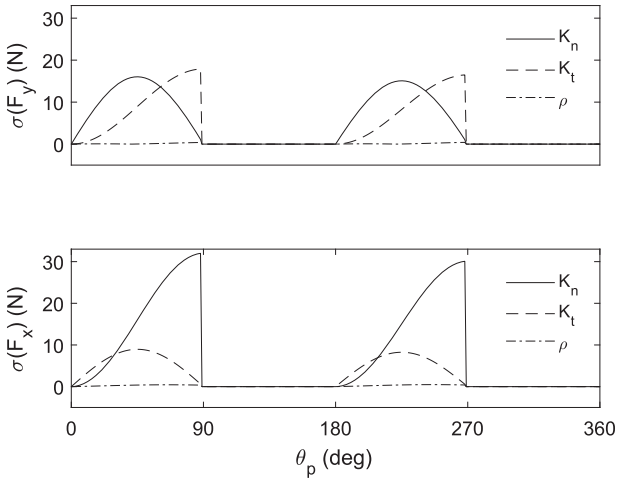

Fig. 11 Relative contributions of variances in cutting coefficients (K_t, K_n) and runout (ρ) to uncertainty in predicted forces using Monte Carlo simulation: feed 0.150 mm/tooth, 50% radial immersion, runout 15 μm, up milling. Other conditions as in Table 5.

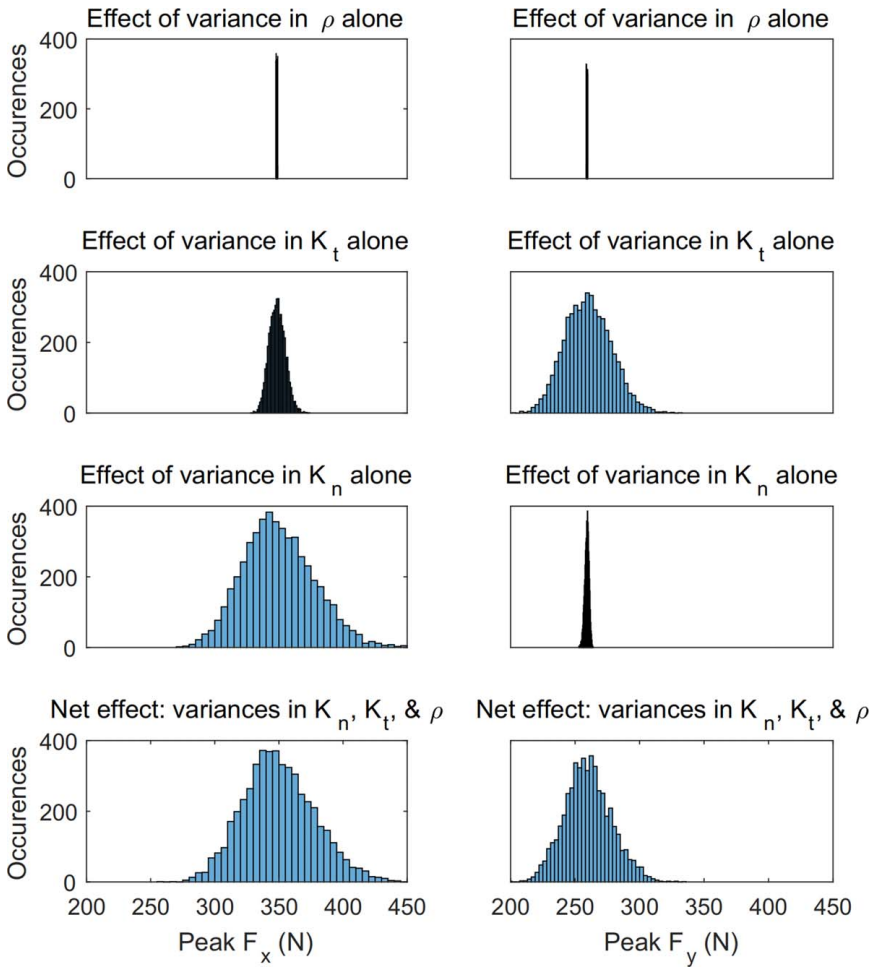

Fig. 12 Contributions of individual variances in cutting coefficients (K_t, K_n) and runout (ρ) on the frequency distribution of peak values of predicted force components using Monte Carlo simulation: feed 0.150 mm/tooth, 50% radial immersion, runout 15 μm, up milling. Other conditions as in Table 5.

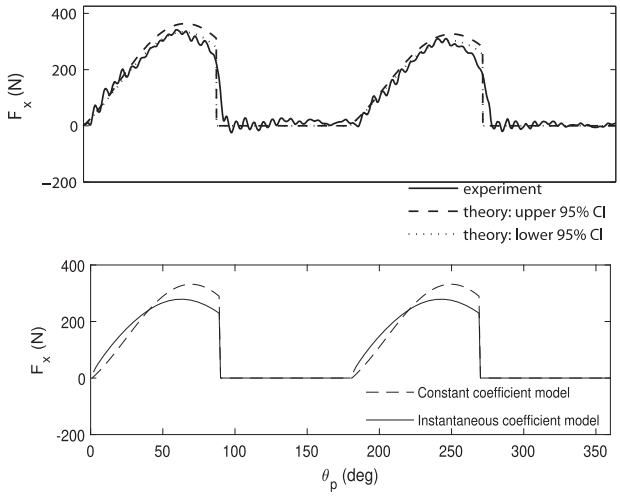

Fig. 13 Model improvement example. Improved prediction of the feed force: feed 0.150 mm/tooth, 50% radial immersion, up-milling. Runout 15 μm. Other conditions as in Table 5. The experimental values of the feed force fall slightly outside the predicted uncertainty band using the constant coefficient model (the top panel). The instantaneous coefficient model predicts the feed force better (the bottom panel).

11 Contributing Factors to Force Prediction Uncertainty

It is interesting to assess the contributions of different factors to the total uncertainty in force prediction. The classical uncertainty procedure and the Monte Carlo procedure offer slightly differing ways of looking at individual contributions.

On the one hand, families of random and systematic effects in various measurements may be viewed as separate contributing factors, and their individual contributions to the total uncertainty may be assessed. This is the nature of information that is obtained from the classical uncertainty procedure presented in this paper. Sources of uncertainty are classified in Table 1. Their individual contributions to the combined uncertainties are quantified and graphically displayed in Fig. 6 for a given set of conditions. A graphical display is convenient because individual contributions are functions of the cutter rotation angle. For instance, in Fig. 6, random effects are seen to dominate individual systematic effects in feed force uncertainty, but the total contribution of the two systematic effects taken together is about the same as that of the random effects.

On the other hand, when applying the Monte Carlo approach, it is convenient to examine the contributions of the variances of individual input parameters, i.e., the two cutting coefficients (equivalently, the four cutting constants), and the radial runout. The simulations can be run by invoking variances of each of these inputs

individually while holding the other factors constant at their mean levels. Several possibilities exist for convenience of visualization of individual contributions. One way is to see the contribution to the standard deviation as a function of cutter rotation angle, an example of which is displayed in Fig. 11. Another way to visualize it is to examine the frequency distribution of the predicted force components at any specific cutter rotation angle for the given number of iterations. An example of this is displayed in Fig. 12 where the cutter rotation angle chosen is that where the individual force component peaks.

12 A Practical Benefit: Model Improvement

A key practical benefit of the uncertainty analysis is that it can point to the shortcomings in the predictive force model itself. Since the predicted forces are no longer single valued, but are predicted to be within a confidence interval, it behooves the actual forces to lie within the predicted band of uncertainty to some reasonable extent. A look at Figs. 8, 9, and 10 reveals that the experimental feed force signals fall slightly outside the prediction interval. This prompts the modeler to refine the model. The constant cutting coefficient model can be replaced with an instantaneous cutting coefficient model since the coefficients are sensitive to the instantaneous chip thickness as shown in the Appendix B. Based on this refined model, the predicted feed forces are seen to better agree with experimental results as shown in Fig. 13.

An even more glaring illustration is displayed in Fig. 14. This example is chosen from Ref. [15] in which a force model was developed for helical endmills, which makes the model more complex than the one used in this paper. When the constant coefficient version of the model was used to predict forces for a certain set of cutting conditions, the experimental force signals were seen to lie fairly outside the predicted 95% confidence interval band for the feed force and the lateral force components as seen in the top panels in Fig. 14. This prompted the modeler to refine the model using instantaneous cutting coefficients.

The improvement in the accuracy of force prediction is quite dramatic as may be seen in Fig. 14. This example also demonstrates the fact that the uncertainty propagation method outlined in this paper is easily applied to any empirical cutting force model. Only the details of the algebraic formulation differ, owing to the individual characteristics of the given model. For instance, in the force model for the helical endmill, the axial component of the force is also considered, which adds to the length of the algebra. The relative complexity of the model, as compared to the straight fluted model, also makes the algebra lengthier. Lest this gives out the impression that the use of instantaneous coefficients is the only way to refine a model, it must be said that there are many ways to do so. For instance, edge coefficients could account for edge roundness effects. The effects of tool wear could be modeled. Modeling is not the objective of this paper. Our proposed method is concerned with the propagation of input uncertainties through any given model. The confidence intervals served to discriminate between the predictive accuracy of the two models in this example.

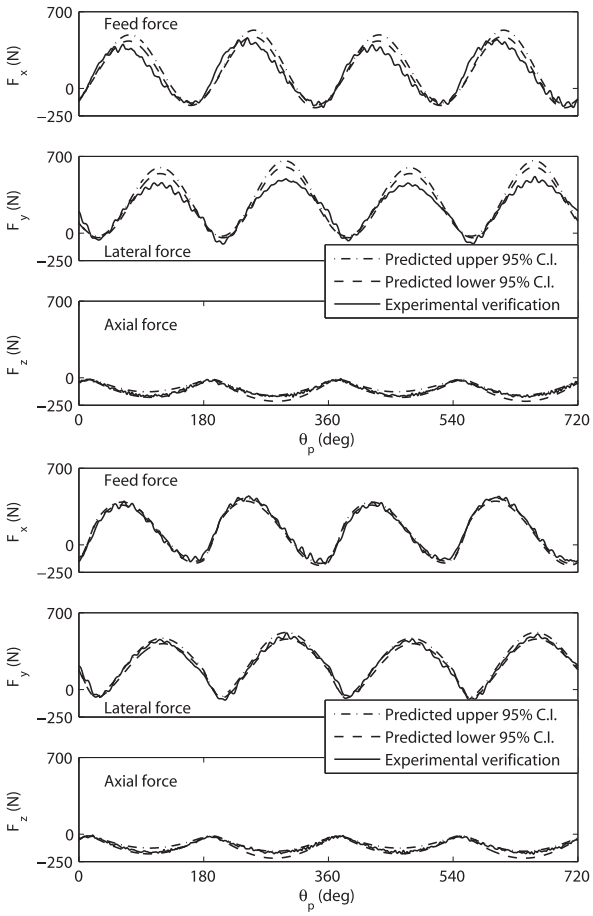

Fig. 14 Illustration of model improvement for a helical endmill prompted by a mismatch between experimental force signals and 95% confidence intervals on model predicted forces. The feed force and lateral force components obtained experimentally are seen to lie outside the predicted confidence intervals to a fair extent in the case of force prediction based on the constant coefficient model (the top three panels). The corresponding model using instantaneous cutting coefficients (the bottom three panels) shows a glaring improvement in predicted feed and lateral forces. Cutting conditions: 45-deg helix endmill, $f_T =$ 0.100 mm/tooth, runout 10 μm, 100% *RI*, slotting an aluminum alloy workpiece: more details available in the corresponding Figs. 9–14 and 10–12 in Ref. [15].

13 Conclusions

An analytical classical uncertainty analysis procedure was applied to the practical problem of determining confidence intervals on predicted cutting forces in end milling. An alternative method of uncertainty analysis based on inferential statistics was also applied using Monte Carlo simulation. This covers a gap in the literature in the field of machining. One application, where cutting force sensing is used for feedback, is the real-time monitoring of tool wear and tool breakages. In comparing the actual cutting forces with predicted (expected) forces, the confidence bounds on the predicted forces need to be considered. One has to be careful in attributing deviations from nominal predicted forces to wear or breakage, when these deviations lie within the confidence regions.

Though the uncertainty analysis was performed for a specific cutting force model applicable for straight-flute endmills, the demonstrated approach is quite general. For other force models, including those for helical endmills, even though the basic force model may differ, the uncertainty analysis procedure would remain the same [15]. This general technique of uncertainty propagation through a milling force model is one of the contributions of this research. The procedure for determining the uncertainties, and the corresponding confidence intervals, is readily implemented. The modeler is able to provide a defensible uncertainty statement to accompany cutting force predictions. This has a practical benefit for the process planner who can decide on the usefulness of model based force predictions in any specific application.

The classical uncertainty analysis is supplemented with an uncertainty analysis procedure based on inferential statistics, namely the Monte Carlo simulation method. This method does not require an involved analytical procedure to determine combined uncertainties. It yields the combined uncertainties directly. Covariances of cutting coefficients were ignored in the Monte Carlo analysis, but it is

possible to do so even in the classical approach. Using covariances yields tighter tolerance bands on confidence intervals.

An important observation is that the force prediction band obtained using the Monte Carlo simulation is not unique. It is only one of an infinite family of such bands so that it will differ somewhat every time one runs the simulation for a given number of iterations. This is a direct function of the specific set of pseudo-random numbers generated each time the simulation is run. This fact does not pose any difficulty compared with the classical uncertainty analysis results. Even in the classical approach, the 95% confidence interval generated is not unique. It is, by definition [16], merely one of a family of intervals in which the value of the cutting force is predicted to lie approximately 95% of the time.

The classical uncertainty analysis requires the algebra to be done, but that is a one time activity. It was shown that this analysis can reveal the impacts of random effects and systematic effects separately. This information can prompt the experimentalist to improve the experimental setup if it is observed that the impact of systematic effects is comparatively very large. On the other hand, a comprehensive analysis to determine combined uncertainties is not warranted when using the Monte Carlo approach because it yields combined uncertainties directly.

Comparison of the predicted force intervals with experimental results shows that the chosen model is a simplified one since portions of the experimental force signals do not always lie within the predicted force intervals. It was shown that this can prompt the modeler to refine the model for more accurate predictions.

Conflict of Interest

There are no conflicts of interest.

Data Availability Statement

The datasets generated and supporting the findings of this article are obtainable from the corresponding author upon reasonable request.

Appendix A: The End Milling Process Description

The endmill (also called the tool or cutter) is held in a toolholder, which is mounted on a powered machine spindle. The workpiece is fed across the tool such that there is a linear relative motion between the endmill and the part, in addition to the rotation of the tool. Material is removed in the form of chips (swarf) via successive passes of cutting edges (teeth) across the workpiece. Endmills have either helical flutes or straight flutes. A force model for straight-flute endmills is considered in this document.

The geometry of peripheral milling with a straight-flute endmill is shown in Fig. 15 which describes the process terminology, namely, the axial depth of cut, b, the radial depth of cut, a_r, the endmill diameter, D, the feed per tooth, f_T, and the spindle speed, Ω. A two-fluted endmill is illustrated. The shape of the uncut chip can also be seen in the sectional view. The radial immersion (RI), expressed as a fraction or a percentage, is defined as the following ratio:

$$\text{Radial immersion, } RI \triangleq \frac{a_r}{D} \tag{A1}$$

Two different types of tooth engagement configuration may be encountered depending upon the direction from which the teeth approach the workpiece. The concept is illustrated in Fig. 16 which shows up-milling and down-milling configurations for RI below 50%. In up-milling, the cut begins with zero chip thickness, whereas in down-milling the cut ends with a zero chip thickness. RI values exceeding 50% result in mixed-mode configurations of two possible types. The cut may either begin with zero chip thickness or end with zero chip thickness. A radial immersion of 100% results in

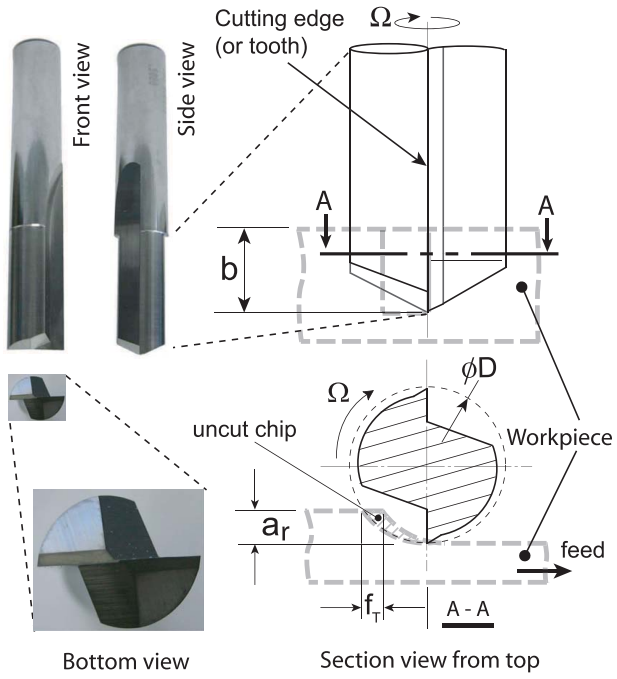

Fig. 15 Geometry of peripheral milling, with a straight-flute endmill, illustrating the axial depth of cut, b, the radial depth of cut, a_r, the endmill diameter, D, the feed per tooth, f_T, and the spindle speed, Ω. The ratio "a_r/D" is defined as the radial immersion (expressed as a fraction or a percentage). The axial depth of cut, b, is also the chip width. A two-fluted endmill is illustrated.

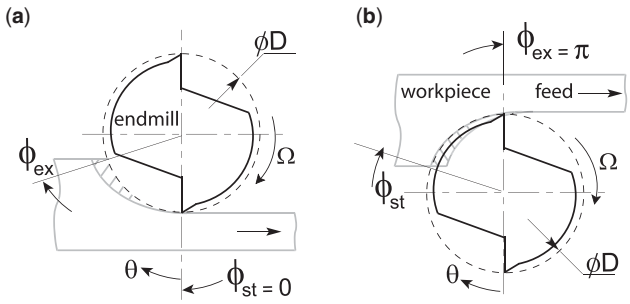

Fig. 16 Cutter-workpiece engagement configurations: (*a*) up-milling and (*b*) down-milling. Both the cases illustrated are for radial immersion below 50%. The tooth engagement angle is designated ϕ. The entry angle is ϕ_{st} and the exit angle is ϕ_{ex}. Total tooth engagement is $(\phi_{ex} - \phi_{st})$.

machining of double-walled channels and is called slotting. Figure 16 also illustrates the entry and exit angles of the tooth in the cut. The angular orientation at which the tooth enters the cut is the entry angle, ϕ_{st}, and the orientation at which it exits the cut is the exit angle, ϕ_{ex}. For a given value of radial immersion, the numerical values of ϕ_{st} and ϕ_{ex} are obtained using simple geometry.

Appendix B: A Cutting Force Model for Straight-Flute Endmills

To demonstrate the propagation of input parameter uncertainty, a very widely used mechanistic model for machining with straight-flute endmills is chosen. This model is proven in the literature [1,4,17–19]. Here, it is described in fair detail for the sake of completeness, as the subsequent uncertainty analysis depends on the structure of this model. Cutting force components are expressed analytically as a function of chip geometry. All other factors,

such as the properties of the workpiece material and tool face friction effects, are included in lumped parameter cutting coefficients, making it an empirical model.

Model of Chip Geometry. Chip geometry depends on the chip width, b, a fixed quantity which equals the axial depth of cut, and the chip thickness, h, a variable quantity which depends on the angular position of the tooth. Martellotti [17] showed that the true path of the milling tooth, in the plane, is trochoidal. His simplified circular tool path approximation yields the chip thickness

$$h(\theta) = f_T \sin\theta \tag{B1}$$

where f_T is the feed per tooth, and θ is the angular orientation at which h is computed.

Force Model for a Single Tooth. For straight-flute cutters, the tangential cutting force, F_t, and the normal cutting force, F_n, on any given tooth are proportional to the uncut chip area, $A_c = bh\ (= b\, f_T \sin\theta)$ [1]. The axial force vanishes, allowing this to be treated as a planar problem. Force components on the pth tooth, as a function of its angular orientation, θ_p, are

$$\begin{Bmatrix} F_t \\ F_n \end{Bmatrix} = \begin{pmatrix} bh & 0 \\ 0 & bh \end{pmatrix} \begin{Bmatrix} K_t \\ K_n \end{Bmatrix} = bf_T \begin{pmatrix} \sin\theta_p & 0 \\ 0 & \sin\theta_p \end{pmatrix} \begin{Bmatrix} K_t \\ K_n \end{Bmatrix} \tag{B2}$$

where K_t and K_n are lumped parameter cutting coefficients which depend on the tool-workpiece-cutting fluid combination, as well as on machining parameters such as cutting speed and chip thickness. They are obtained by experiment for any specific situation. K_t and K_n are called the tangential and normal cutting coefficients, respectively.

Transforming to a fixed frame of reference (Fig. 17) we have, for the force components, when the tooth is in the cut (i.e., when $\theta_p \in [\phi_{st}, \phi_{ex}]$)

$$\begin{Bmatrix} F_x \\ F_y \end{Bmatrix} = \frac{bf_T}{2} \begin{pmatrix} \sin 2\theta_p & 1-\cos 2\theta_p \\ 1-\cos 2\theta_p & -\sin 2\theta_p \end{pmatrix} \begin{Bmatrix} K_t \\ K_n \end{Bmatrix} \tag{B3}$$

and $F_{x,y} \equiv 0$ when $\theta_p \notin [\phi_{st}, \phi_{ex}]$ (tooth out of the cut).

Average Force-Based Estimate of K_t and K_n. Sabberwal [19] showed that the mean cutting coefficient could be related to the average values of the cutting force. For a single tooth, the averaged components of the cutting force, $\overline{F}_x$, and $\overline{F}_y$, may be expressed as

$$\begin{Bmatrix} \overline{F}_x \\ \overline{F}_y \end{Bmatrix} = \left[\frac{bf_T}{2(\phi_{ex}-\phi_{st})} \int_{\phi_{st}}^{\phi_{ex}} \begin{pmatrix} \sin 2\theta_p & 1-\cos 2\theta_p \\ 1-\cos 2\theta_p & -\sin 2\theta_p \end{pmatrix} d\theta_p \right] \times \begin{Bmatrix} K_t \\ K_n \end{Bmatrix} \tag{B4}$$

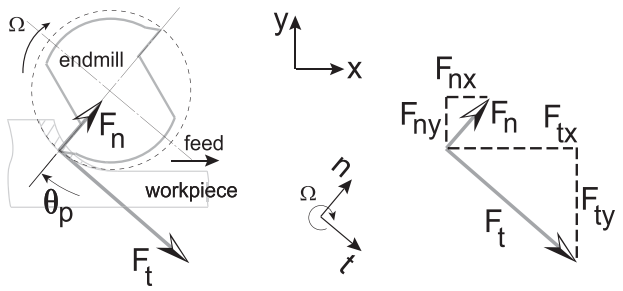

Fig. 17 Transformation of forces from a rotating frame (*t*, *n*) to a fixed frame (*x*, *y*)

Upon simplification

$$\begin{Bmatrix} \overline{F}_x \\ \overline{F}_y \end{Bmatrix} = \frac{bf_T}{2(\phi_{ex}-\phi_{st})} \begin{pmatrix} \mu & \nu \\ \nu & -\mu \end{pmatrix} \begin{Bmatrix} K_t \\ K_n \end{Bmatrix} \tag{B5}$$

where, for convenience, μ and ν are shorthand for the following expressions:

$$\begin{aligned} \mu &= \sin(\phi_{st}+\phi_{ex})\sin(\phi_{ex}-\phi_{st}) \\ \nu &= (\phi_{ex}-\phi_{st}) - \cos(\phi_{st}+\phi_{ex})\sin(\phi_{ex}-\phi_{st}) \end{aligned} \tag{B6}$$

Inverting

$$\begin{Bmatrix} K_t \\ K_n \end{Bmatrix} = \frac{2(\phi_{ex}-\phi_{st})}{bf_T(\mu^2+\nu^2)} \begin{pmatrix} \mu & \nu \\ \nu & -\mu \end{pmatrix} \begin{Bmatrix} \overline{F}_x \\ \overline{F}_y \end{Bmatrix} \tag{B7}$$

where the average force components are obtained from experiments, and all other terms on the right-hand side of the above equation are known.

Multiple Tooth Formulation. For a multiple tooth cutter, individual force signatures due to each tooth are qualitatively identical, except that they are phase shifted by a suitable pitch angle with respect to the reference (pth) tooth, and differ in magnitude since the associated effective feed per tooth differs due to radial runout or differential pitch effects. The components of the total force on the endmill, $F_{X,Y}$, are a summation of the appropriately phase shifted force components of the individual teeth.

Average Chip Thickness. Martellotti [17] proposed that the average undeformed chip thickness could be related to the components of the cutting force. The concept of average chip thickness is invoked to facilitate the experimental determination of cutting coefficients, as well as average cutting forces. Using Eq. (B1), the average chip thickness is

$$\overline{h} = \frac{1}{\phi_{ex}-\phi_{st}} \int_{\phi_{st}}^{\phi_{ex}} f_T \sin\theta\, d\theta = \frac{f_T(\cos\phi_{st}-\cos\phi_{ex})}{\phi_{ex}-\phi_{st}} \tag{B8}$$

Cutting Coefficient Models. For fixed levels of cutting speed and axial depth of cut, the cutting coefficients depend on the the chip thickness. A logarithmic relationship of the general form $K = e^{\Gamma}(\overline{h})^{\Psi}$, proposed by Sabberwal [19] is adopted, leading to

$$\begin{Bmatrix} \ln K_t \\ \ln K_n \end{Bmatrix} = \begin{pmatrix} 1 & \ln\overline{h} & 0 & 0 \\ 0 & 0 & 1 & \ln\overline{h} \end{pmatrix} \begin{Bmatrix} \Gamma_t \\ \Psi_t \\ \Gamma_n \\ \Psi_n \end{Bmatrix} \tag{B9}$$

where $\Gamma_{t,n}$ and $\Psi_{t,n}$ are cutting constants whose values depend on the combination of tool material and work material, the specific cutting geometry, as well as cutting conditions, such as the type of cutting fluid being used. The coefficients also depend on other process parameters such as cutting speed and axial depth of cut.

The cutting coefficient model described above is based on the averaged chip thickness but the coefficients are sensitive to the instantaneous value of the chip thickness. A more refined model uses the instantaneous chip thickness to calculate instantaneous cutting coefficients. The general form of such a relationship is $K = e^{\Gamma}(f_T \sin\theta)^{\Psi}$.

Modeling the Tooth Runout Effects. Kline and DeVor [20] identified the effect of runout on the cutting force system. The radial runout influences the effective feed rate experienced by an individual tooth. A static measurement of runout can be taken using a dial indicator. The total indicated reading (TIR) can be used as a measure of the radial runout. The relative runout between successive teeth, ρ, governs the effective feed experienced

by each tooth. For a two-fluted cutter, the effective feed rates, f_{Ti}, on individual teeth are

$$f_{T1} = f_T + |\rho| \quad \text{and} \quad f_{T2} = f_T - |\rho| \tag{B10}$$

For a cutter with more than two teeth, the expressions for effective feed can be derived using similar arguments.

References

[1] Tlusty, J., 2016, *Manufacturing Processes and Equipment*, 7th ed., Prentice Hall, Boston, MA.

[2] Mann, B. P., Young, K. A., Schmitz, T. L., and Dilley, D. N., 2005, "Simultaneous Stability and Surface Location Error Predictions in Milling," ASME J. Manuf. Sci. Eng., **127**(3), pp. 446–453.

[3] Nemes, J. A., Asamoah-Attiah, S., Budak, E., and Kops, L., 2001, "Cutting Load Capacity of End Mills With Complex Geometry," CIRP. Ann., **50**(1), pp. 65–68.

[4] Ehman, K. F., Kapoor, S. G., DeVor, R. E., and Lazoglu, I., 1997, "Machining Process Modeling: A Review," ASME J. Manuf. Sci. Eng., **119**(4B), pp. 655–663.

[5] Kurdi, M. H., 2005, "Robust Multicriteria Optimization of Surface Location Error and Material Removal Rate in High Speed Milling Under Uncertainty," PhD thesis, University of Florida, Gainesville, FL.

[6] Duncan, S. S., Kurdi, M. H., Schmitz, T. L., and Snyder, J. P., 2006, "Uncertainty Propagation for Selected Analytical Milling Stability Limit Analyses," Transactions of NAMRI/SME, Milwaukee, WI, Society of Manufacturing Engineers (SME), pp. 17–24.

[7] Taylor, B. N., and Kuyatt, C. E., 1994, *NIST* Technical Note 1297, 1994 edition: Guidelines for Evaluating and Expressing the Uncertainty of NIST Measurement Results. United States Department of Commerce Technology Administration, National Institute of Standards and Technology, Gaithersburg, MD.

[8] ISO, 1995, Guide to the Expression of Uncertainty in Measurement, 2nd ed. International Organization for Standardization, Geneva.

[9] Kacker, R., Sommer, K. D., and Kessel, R., 2007, "Evolution of Modern Approaches to Express Uncertainty in Measurement," Metrologia, **44**(6), pp. 513–529.

[10] Zellner, A., 1962, "An Efficient Method of Estimating Seemingly Unrelated Regressions and Tests for Aggregation Bias," J. Am. Stat. Assoc., **57**(298), pp. 348–368.

[11] Cadille, R., 2008, *Manufacturer's Certificate*, Kistler Instrument Corp., Amherst, NY.

[12] Turzeniecka, D., 2000, "Errors in the Evaluation of the Coverage Factor as a Criterion of Applications of Approximate Methods of Evaluation of Expanded Uncertainty," Measurement, **27**(4), pp. 223–229.

[13] Fotowicz, P., 2006, "An Analytical Method for Calculating a Coverage Interval," Metrologia, **43**(1), pp. 42–45.

[14] Willink, R., 2007, "A Generalization of the Welch–Satterthwaite Formula for Use With Correlated Uncertainty Components," Metrologia, **44**(5), pp. 340–349.

[15] Bhattacharyya, A., 2008, "Predictive Force Modeling of Peripheral Milling," PhD thesis, University of Florida, Gainesville, FL.

[16] Ott, R. L., and Longnecker, M., 2000, *An Introduction to Statistical Methods and Data Analysis* (Cengage Learning), Upper Saddle River, NJ.

[17] Martellotti, M., 1941, "An Analysis of the Milling Process," Trans. ASME, J. Eng. Industry, **63**, pp. 667–700.

[18] Kline, W., 1982, "The Prediction of Cutting Forces and Surface Accuracy for the End Milling Process," Ph.D. thesis, University of Illinois, Champaign, IL.

[19] Sabberwal, A., 1961, "Chip Section and Cutting Force During the Milling Operation," CIRP. Ann., **10**(1), pp. 197–203.

[20] Kline, W. A., and DeVor, R. E., 1983, "The Effect of Runout on Cutting Geometry and Forces in Endmilling," Int. J. Mach. Tool Des. Res., **23**(2–3), pp. 123–140.